The Cryosphere Discuss., 8, 3171–3206, 2014
www.the-cryosphere-discuss.net/8/3171/2014/
doi:10.5194/tcd-8-3171-2014

The Cryosphere Discussions
Open Access

A novel integrated method to describe dust and fine supraglacial debris and their effects on ice albedo: the case study of Forni Glacier, Italian Alps

R. S. Azzoni[1], A. Senese[1], A. Zerboni[1], M. Maugeri[2], C. Smiraglia[1], and G. A. Diolaiuti[1]

[1]Università degli Studi di Milano, Dipartimento di Scienze della Terra "A. Desio", Milan, Italy
[2]Università degli Studi di Milano, Dipartimento di Fisica, Milan, Italy

Received: 31 January 2014 – Accepted: 14 May 2014 – Published: 13 June 2014

Correspondence to: A. Senese (antonella.senese@unimi.it)

Published by Copernicus Publications on behalf of the European Geosciences Union.

Abstract

We investigated the characteristics of sparse and fine debris coverage at the glacier melting surface and its relation to ice albedo. In spite of the abundant literature dealing with dust and black carbon deposition on glacier accumulation areas (i.e.: on snow and firn), few studies that describe the distribution and properties of fine and discontinuous debris and black carbon at the melting surface of glaciers are available. Furthermore, guidelines are needed to standardize field samplings and lab analyses thus permitting comparisons among different glaciers. We developed a protocol to (i) sample fine and sparse supraglacial debris and dust, (ii) quantify their surface coverage and the covering rate, (iii) describe composition and sedimentological properties, (iv) measure ice albedo and (v) identify the relationship between ice albedo and fine debris coverage. The procedure was tested on the Forni Glacier surface (northern Italy), in summer 2011, 2012 and 2013, when the fine debris and dust presence had marked variability in space and time (along the glacier tongue and from the beginning to the end of summer) thus influencing ice albedo: in particular the natural logarithm of albedo was found to depend on the percentage of glacier surface covered by debris. Debris and dust analyses indicate generally a local origin (from nesting rockwalls) and the organic content was locally high. Nevertheless the finding of some cenospheres suggests an anthropic contribution to the superficial dust as well. Moreover, the effect of liquid precipitation on ice albedo was not negligible, but short lasting (from 1 to 4 day long), thus indicating that also other processes affect ice albedo and ice melt rates and then some attention has to be spent analysing frequency and duration of summer rainfalls for better describing albedo and melt variability.

TCD
8, 3171–3206, 2014

1 Introduction

1.1 Research motivation and study aims

Debris generally affects glaciers and glacierized areas and influences their features and evolution in a great variety of ways (Bolch, 2011). In fact, debris can be found: (i) at the surface of glaciers (i.e.: supraglacial debris), (ii) within glaciers (i.e.: englacial debris), (iii) at the ice–bedrock interface (i.e.: subglacial debris), and (iv) outside the glaciers, at their boundaries (i.e.: lateral and frontal moraines). As a consequence, it influences the glacier system in a non-negligible way; the most important and well-known effect of debris in glacierized areas is on glacier ablation. A valuable example of debris cover effect on ablation is found on actual debris-covered glaciers (see Kirkbride, 2011). In fact, there are many studies dealing with supraglacial debris role in driving magnitude and rate of buried ice ablation depending on its depth (Ostrem, 1959; Nakawo and Young, 1981, 1982; Nakawo and Rana, 1999; Tangborn and Rana, 2000; Sakai et al., 2000; Deline, 2005; Nicholson and Benn, 2006). Debris cover, whenever thicker than a "critical thickness" (sensu Mattson et al.,1993), reduces the magnitude and rate of buried ice melt with respect to bare ice at the same elevation. The critical thickness value has to be locally evaluated and mainly depends on rock lithology and grain size and on the geographical glacier setting (Mihalcea et al., 2006, 2008a, b; Diolaiuti et al., 2009). Moreover, in recent times dust and black carbon deposition on glacier accumulation areas (at the surface of snow and firn) are of increasing interest to the scientific community due to enhanced snow melting rates affecting glaciers in the high elevation glacierized areas of Asia (Flanner et al., 2009; Yasunari et al., 2010).

In spite of this abundant literature dealing with (i) thicker and quite continuous debris layer at the glacier melting surface (this is the case of actual debris covered glaciers and glacier medial moraines), and (ii) fine debris deposition on glacier accumulation areas, the effects of fine (mainly dust) and sparse debris cover at the melting surface of debris-free glaciers (with this term we indicate glaciers not characterized by an

TCD
8, 3171–3206, 2014

extensive and quite continuous debris coverage) are still poorly debated and sometimes underestimated.

Then in this contribution we show the results from our researches devoted to quantify fine debris coverage at the melting surface of an alpine debris-free glacier to evaluate its seasonal variability and its influence on ice albedo. Moreover, to permit comparisons between different glacier zones and among different glaciers, we also developed a protocol to standardize field and lab analyses.

We also focus our attention on the development of fine supraglacial debris, in order to estimate the evolution of the sedimentological properties and the debris coverage rate during the melting season. Furthermore, we assess the influence of a rainfall event on the changes of fine supraglacial debris distribution and consequently on ice albedo.

1.2 Previous studies and recent literature on supraglacial fine debris

One of the most important glacier albedo driving factor (apart from, for the instance, the meteorological conditions and the light scattering by bubbles and cracks) is the light absorption by fine debris and dust (Brock et al., 2000; Brock, 2004; Klok et al., 2003), which vary across the glacier surface both in space and in time.

Supraglacial fine debris and dust consist of mineral and organic fractions. Both components may be autochthonous or allochthonous. The organic elements can be originated from bacterial decomposition of organic matter (in situ or outside the glacier), or they can consist of black carbon (e.g.: deriving from fossil combustion and fires) and organic remains in aerosols (Fujita, 2007; Takeuchi et al., 2001; Takeuchi, 2002). On the one hand the mineral fraction can be locally derived from the weathering of rock outcrops and nunataks or from lateral moraines and debris slopes: in fact, during the summer when warm climatic conditions occur, the dry and unconsolidated materials constituting moraines are easily transported by wind gusts and deposited tens to hundreds of meters away (Oerlemans, 2009). On the other hand, the dust and fine debris can be transported for long distances by atmospheric circulation from non-glaciated areas (Ming et al., 2009; Ramanathan, 2007). For instance, the deposition of Saharan

TCD
8, 3171–3206, 2014

dust (Sodermann et al., 2006) or volcanic ash (Conway et al., 1996) on glaciers are well-known phenomena and are also largely known the darkening processes which are affecting the largest part of Alpine debris-free glaciers (e.g., Oerlemans et al., 2009; Paul and Kääb, 2005; Paul et al., 2007; Diolaiuti and Smiraglia, 2010; Painter et al., 2013) thus changing their albedo and affecting melt magnitude and rates.

In fact, to distribute the glacier energy budget for assessing ice melt at the surface of debris-free glaciers, the choice of a correct ice albedo value is critical and the albedo parameterizations used in energy and mass balance models are often inadequate to represent spatial and temporal changes in the surface albedo and are consequently regarded as a major source of errors (e.g. Arnold et al., 1996; Klok and Oerlemans, 2002; Klok et al., 2003).

Therefore studies which combine measurements of supraglacial fine debris cover and dust distribution and features with systematic measurements of glacier albedo are needed.

On the one hand some authors have deeply investigated dust deposition on snow-pack (e.g.: Qian et al., 2011; Yasunari et al., 2010). A possible snow albedo reduction due to black carbon contamination was revealed by radiation measurements at the snow surface performed at Barrow, Alaska (Aoki et al., 1998, 2002) and in Japanese urban areas (Motoyoshi et al., 2005). In the case of snow and firn, a field procedure was developed, followed by further standardized lab-analyses to quantify and describe black carbon presence and features (Yasunari et al., 2010).

On the other hand minor attention was paid on fine debris and dust deposition at the glacier melting surface. A first attempt to parameterize not only snow albedo variability but also the ice one on a debris-free glacier was performed by Brock et al. (2000). In spite of the good results they obtained analysing snow covered area, less accurate was the evaluation of debris cover impact on ice albedo. In fact the debris cover was assessed with the aid of a 0.5 m^2 quadrat and investigated through two surrogates (i.e. cumulative melt and number of days, both calculated since exposure of the ice surface). From this study arose the need for further researches to standardize the measurements

TCD
8, 3171–3206, 2014

of supraglacial fine debris and dust at the glacier ice surface thus avoiding the use of surrogates unable to full describe debris coverage and its seasonal variability.

2 Study area

Our experiments were carried out on the ablation tongue of the Forni Glacier (Fig. 1), the widest Italian valley glacier featuring a surface area of 11.34 km^2 (2007 data, Garavaglia et al., 2012). It is located in the Ortles-Cevedale Group, Stelvio National Park, Lombardy Alps. It is widely debris-free, even if darkening phenomena are ongoing (D'Agata et al., 2013) and some authors have recently pointed out that fine and sparse debris is becoming abundant due to the ongoing glacier shrinkage (Diolaiuti and Smiraglia, 2010; Diolaiuti et al., 2012; Senese et al., 2012a). For this reason, the Forni Glacier can be considered a good laboratory to evaluate fine and sparse debris distribution and seasonal evolution and its influence on ice albedo. The Forni Glacier has a northward down-sloping surface; it is about 3 km long and its altitude ranges from 2600 m to about 3670 m a.s.l. Metamorphic rocks, mostly micaschist rich in quartz, muscovite, chlorite and sericite, constitute the dominant lithology (Montrasio et al., 2008); these rocks emerge from the glacier surface as nunataks (mainly in the accumulation basins) and as rock outcrops (surrounding the glacier tongue). These latter are increasing in size and becoming very frequent due to the ongoing glacier retreat and thinning phase (Diolaiuti and Smiraglia, 2010; Diolaiuti et al., 2012).

Studies on short term changes of the Forni Glacier have been performed through an Automatic Weather Station (named AWS1 Forni) running from 2005 at the glacier melting surface. The AWS1 Forni is already included in the international meteorological network SHARE (Stations at High Altitude for Research on the Environment) managed by EvK2CNR and in the CEOP network (Coordinated Energy and Water Cycle Observation Project), promoted by WCRP (World Climate Research Programme) within the framework of the GEWEX project (Global Energy and Water Cycle Experiment). It is also the unique Italian site inserted in the SPICE (Solid Precipitation Intercomparison

TCD
8, 3171–3206, 2014

Experiment) project managed and promoted by WMO (World Meteorological Organization). The AWS1 Forni is located on the ablation tongue (c. 2631 m a.s.l.), about 800 m from the glacier terminus, and it is equipped with sensors for measuring air temperature and humidity, wind speed and direction, atmospheric pressure, liquid precipitation and snow depth, and longwave and shortwave radiation, both incoming and outgoing (Citterio et al., 2007; Diolaiuti et al., 2009; Senese et al., 2010, 2012a, b).

3 Methods

In the time frame 2011–2013 we performed totally 51 field measurements on the debris-free ablation tongue of the Forni Glacier (Fig. 1): both debris quantification (i.e.: spatial distribution) and albedo evaluation (Fig. 2). Moreover, we sampled the supraglacial debris/dust (totally 13 surveys) to assess the debris coverage rate (C_r from here) and the sedimentological features (i.e. grain size, humified and total organic carbon and mineralogical properties). The sites for field measurements were chosen considering: (i) homogeneity in debris cover, (ii) presence or absence of fine sparse debris, (iii) diverse debris grain size, and (iv) different distances from rock slopes and medial moraines, which are the main debris suppliers, thus assuring that the selected sites are representative of the range of surfaces present at the glacier melting area. Moreover the choice of each sampling parcel of area 1 m × 1 m was made selecting the ones which show features common to the as wide as possible area nearby: in this way the analyses performed at each single parcel provided results valid for the surrounding zone as well. The medial moraines were excluded from this work because we only focused on fine and sparse debris covered ice and not on actual buried ice (i.e.: ice covered by a thick and quite continuous debris layer). Figure 1 shows the study area and the positions of the sites we analysed.

TCD
8, 3171–3206, 2014

3.1 Debris cover quantification

The quantification of supraglacial sparse and fine debris and dust was performed by acquiring high resolution digital images at each analysed site (Fig. 2c) and processing them with image analysis software *ImageJ* following Irvine-Fynn et al. (2010) (Fig. 3). Digital RGB (red-green-blue, in colour composite) photographs of the 1 m × 1 m parcel were taken using a digital camera (Nikon D40, 6.1 megapixels). From a total of 445 images, we selected one for each measurement site (totally 51): those affected by shadows, deformations, photographic imperfections (e.g. poor exposure, incorrect focus) were excluded from the analysis and only images showing clear differences between bare ice and dust/fine debris-covered ice were considered.

The selected images were first cropped delimiting the 1 m × 1 m parcel (Fig. 3a). Second, we converted them to 8 bit greyscale in order to highlight the contrast between glacier ice and debris/dust. Third, as a darker grey pixel denotes the presence of debris or shadow (the latter due to surface roughness), we assumed that debris granules could be isolated by thresholding for those pixels with brightness values which fall below a specified GrayScale Threshold level (T_{GS} from here, Fig. 3b) was specified by a supervised classification. In particular the threshold was iteratively adjusted until the isolated image pixels best coincide with the debris/dust (Fig. 3c). An 8 bit image is composed of 256 grey tones ranging from 0 (black) to 255 (white) and ice surfaces can be isolated by selecting the pixels with brightness values higher than a specified T_{GS}; for instance, if the T_{GS} value is fixed at 100, pixels with a grey tones from 0 to 100 represent debris and pixels with a grey tone from 101 to 255 represent ice. For each image the pixels with a value lower than T_{GS} were turned into black colour and the other ones into white colour (Fig. 3d). Finally the ratio of the surface covered by debris (d from here) was obtained as:

$$d = \frac{\text{number of black pixels}}{\text{total number of pixels}} \quad (1)$$

TCD
8, 3171–3206, 2014

In order to investigate the robustness of this method for quantifying the ratio of glacier surface covered by debris (d) and in particular to evaluate its sensitivity to changes in the threshold, we performed some tests: (i) we varied the chosen T_{GS} up to ±10 % of its initial value ($T_{GS+10\%}$ and $T_{GS-10\%}$, respectively) and (ii) we averaged all the chosen T_{GS} thus obtaining a unique value ($T_{GS\text{-}AVE}$). All these thresholds ($T_{GS+10\%}$, $T_{GS-10\%}$ and $T_{GS\text{-}AVE}$) were applied to each image for re-calculating the ratio of surface covered by debris (i.e. $d_{+10\%}$, $d_{-10\%}$ and d_{AVE} respectively) and the results were compared to the ones derived from the chosen T_{GS} data.

3.2 Albedo

The albedo (α) is defined as the broadband hemispherically averaged reflectance in approximately the spectral range 0.3–2.8 µm (Brock et al., 2000) and depends on solar elevation, cloudiness, presence of liquid water, crystal structure, ice surface conditions and the presence or absence of coverage (rock debris, dust, organic matter, etc.). This parameter can range from 0 (all the SWin is absorbed by the surface) to 1 (all the SWin is reflected). It is estimated as the ratio of measured outgoing shortwave (SW_{out}) to measured incoming shortwave (SW_{in}):

$$\alpha = \frac{SW_{out}}{SW_{in}} \quad (2)$$

For this study the albedo was calculated from radiation data measured using two pyranometers (the ones installed in the net radiometer CNR1, Kipp&Zonen; see Fig. 2). The sensor features an accuracy of ±5 %. The net radiometer was equipped with a waterproof box containing a data logger, a 5 Ah battery and a 10 W solar panel on the lateral face. Moreover, a tripod was used to raise the net radiometer for short periods (c. 20–30 min for each measurement) above the ice surface. Tests regarding the influence of the height of the sensor above the surface on albedo values were performed, installing the sensor at various distances from the surface. Since we chose sites featuring homogeneous surfaces, we did not find appreciable differences between albedo

TCD
8, 3171–3206, 2014

values measured at the same site thus suggesting a negligible influence of the sensor height.

The CNR1 net radiometer was chosen for its accuracy and resolution in measuring shortwave radiation and it is also the same type as the one running at the AWS1 Forni (Citterio et al., 2007; Senese et al., 2012a) thus assuring the comparability among the two datasets. Then the radiation data collected using the portable instrument were crosschecked and analysed against the data acquired by the AWS1 Forni. The radiation measurements were carried out following the guidelines of the WMO (2008).

The radiation data were acquired every second, and every minute the minimum, average, maximum and standard deviation values were calculated. Albedo measurements were taken in the central hours of the clear-sky day (i.e. from 11 a.m. to 3 p.m., when the solar incidence angles are smaller), thus ensuring the albedo calculations were more accurate and reliable (Brock et al., 2000; Brock, 2004; Oerlemans, 2010). The mean geographic coordinates (WGS84 datum) for each measurement site were recorded by a GPS receiver and the characteristic features of the local ice surface were also noted. Fifty-one measurements were carried out from the beginning of the ice ablation period (when snow coverage at the melting tongue disappeared, exposing ice to solar radiation and dust/debris deposition) to the end of the ice melting season (before the occurrence of the first snow fall event covering the glacier ice and preventing dust/debris deposition): 30 June and 25 August 2011, 4 July, 7 August and 9 September 2012, and 31 July and 6 September 2013.

Moreover we also analysed the effect of liquid precipitation on glacier albedo variability. In fact the liquid precipitation washes out the finer sediment above glacier ice surface (Oerlemans, 2009) thus changing ice albedo. This water effect was quantified by comparing albedo values before, during and after the occurrence of actual liquid precipitation. We considered an actual rainfall any event occurred whenever the hourly air temperature was higher than 1.5 °C (Senese et al., 2012a) and featuring an hourly liquid precipitation stronger than 0.2 mm. The precipitation temporal length (i.e. number

TCD
8, 3171–3206, 2014

of rainy days) and amount (i.e. mm of rain) were measured by a rain gauge installed at the AWS1 Forni.

3.3 Sedimentological analyses and debris coverage rate evaluation

Several bulk samples of supraglacial sediment were collected from the glacier surface (Fig. 2a) and divided into sub-samples for physical and chemical analyses. First in 2011 the eight samples enabled characterization of the spatial variability of supraglacial debris. Then in 2012 (4 July, 7 August and 9 September) we focused our attention on the temporal evolution of debris features by sampling three sites (identified by ablation stakes) with different conditions of supraglacial debris cover: samples 9a, 9b and 9c fine and sparse sediment (1), samples 10a, 10b and 10c widespread debris cover (2) and samples 11a, 11b and 11c coarse debris (3). Finally, in 2012 and 2013 we assessed the debris coverage rate (C_r). In the last year the samples were collected 4 times (samples 12a, 12b, 12c, 12d): 11 July, 31 July, 6 September and 4 October.

Each sampling was carried out by scraping the glacier surface with a cleaned chisel, completely removing the surface layer (from 2 to 5 cm deep); the collected material was preserved in appropriate holders. A cold chain (ice boxes) was used to preserve sediment samples at cold temperature conditions (lower than +4 °C) during transport to the laboratory, where further analyses were carried out.

For evaluating the debris coverage rate (C_r), debris samples were periodically collected from the same sites. First it was necessary to clean the parcel of 1 m × 1 m of area completely removing surface debris (i.e.: scraping at least 2 cm of surface ice). Second, about one month later, the sampling of the surface sediments was repeated on the same glacier parcel which was marked on the field to be retrieved. Then in the lab debris samples were dried and weighted. The ratio between the weight of the debris deposited at the ice surface (in grams) and the time frame occurred (days) permitted

TCD
8, 3171–3206, 2014

to evaluate the debris coverage rate (C_r in g day^{-1}):

$$C_r = \frac{\text{sample weight}}{\text{time frame}} \quad (3)$$

The samples collected in 2011 and 2012 for evaluating the spatial and temporal variability were subject to the analytical procedures summarized as follows. Grain size analyses (Gale and Hoare, 1991) were performed after removing organics using hydrogen peroxide (130 vol) treatment; sediments were wet sieved (diameter from 1000 to 63 mm), then the finer fraction (63 mm) was determined by aerometer on the basis of Stokes's law. Humified organic carbon was identified by means of the Walkley and Black (1934) method, using chromic acid to measure the oxidizable organic carbon (titration). Total organic carbon (TOC) was estimated by loss on ignition (LOI; Heiri et al., 2001), with an uncertainty margin of ±0.1 %; samples were air-dried and organic matter was oxidized at 500–550 °C to carbon dioxide and ash, then the weight lost during the reaction was measured by weighing the samples before and after heating.

Additionally, we performed several XRD (X-Ray Diffraction) and SEM (Scanning Electron Microscope) analyses on randomly oriented powder from the bulk debris samples to investigate the mineralogical properties of the fine debris and dust and the occurrence of micro features (e.g: pollen, spores, micro fauna, algae, etc.).

4 Results

4.1 Debris coverage ratio (d) and ice albedo (α)

The image analysis permitted to evaluate 51 d values ranging from 0.01 to 0.63 (Fig. 4). The ice albedo acquired by the net portable radiometer was found varying from 0.06 to 0.32.

The two data records (i.e. d and α) result highly correlated. The plot showing the natural logarithm of ice albedo ($\ln\alpha$, y-axis) vs. d values (x-axis) is reported in Fig. 5.

TCD
8, 3171–3206, 2014

The regression line is given by:

$$\ln \alpha = (-2.04 \pm 0.19) \cdot d + (-1.50 \pm 0.04) \quad (4)$$

The correlation is 0.84 (the 95 % coefficient interval ranging from 0.74 to 0.91).

The most frequent d value we found was 0.03 but our dataset suggests a wide variability of surface features and then the needing for accurate and numerous surveys at the surface of an Alpine glacier devoted to describe d pattern and then albedo distribution.

To assess the most suitable d value to differentiate a completely debris-free ice surface from a partially debris-covered one, some attempts were performed. In fact it is almost impossible to find a melting glacier surface completely free from dust and/or debris (Oerlemans et al., 2009), thus suggesting that a null d value (i.e. 0 % of debris in a 1 m^2 parcel) is unrealistic. Then we considered the pictures featuring a typical ice albedo (i.e. 0.3–0.4) and we compared their d values. We found that a d value lower than 0.06 (i.e. 6 % of debris coverage over a 1 m × 1 m parcel) represents a debris-free surface.

Regarding the impact of liquid precipitation on supraglacial fine debris and ice albedo, we report in Table 1 the mean daily albedo values before, during and after rainfall events. First, the days before the rainfall featured a mean daily albedo equal to 0.22. Second, whenever a precipitation occurred the mean daily reflectivity was reduced to 0.20 due to the water albedo being lower than ice (i.e. equal to 0.05–0.10, Hartmann, 1994). This phenomenon was found occurring over 18 events of a total number of 30: as regards the remained 12 cases, 6 featured an albedo increase and 6 steady state albedo conditions. This variable trend can be attributed to the rain amount: in fact a misty rain decreases the surface albedo less than a heavy liquid precipitation. Third once the rain event has washed out the dust, the mean daily albedo resulted 0.26. Almost all rain events (28 over a total number of 30) showed a mean daily albedo increase slightly higher than 20 %. On the contrary when albedo before the rainfall was

TCD
8, 3171–3206, 2014

higher than 0.30, the water effect was not so appreciable. In fact this reflectivity value is typical of the bare ice with no debris coverage.

The occurrence of the washing out effect and the consequent reflectivity increase was found to be short lasting. The mean time period to restore the previous albedo value result equal to 1.8 days (ranging from 1 to 4 days) occurring over 10 events over a total of 30. Whenever the interval between two rainfalls was equal to 1 day, the albedo was higher than following the previous rain event (51 % of the analysed events).

4.2 Debris features and debris coverage rate (C_r)

The spatial variability of the fine debris cover is highlighted from 2011 data. The sediment analysis performed in the lab indicates significant variability in the total organic carbon (TOC, from 0.6 % to 5.9 %, see Table 2). The highest content of organic matter was found in samples 5, 6 and 8; in particular, sample 5 was wholly cryoconite, where generally the development of algae and bacteria communities is extremely favoured (Takeuchi et al., 2000, 2005). The lowest value of total organic carbon was found in sample 2, which was collected on a glacier area located close to the flank of the nesting rock walls, a site which receives a high amount of debris originating from macrogelivation and weathering processes. Rock debris coverage here is younger (recent deposition) and unstable, and therefore poorly colonized by supra-glacial organisms. Moreover, the grain-size analysis shows that samples collected at these sites are characterized by coarser sediments, in keeping with their origin, mostly due to slope erosion.

Regarding the debris origin, X-ray diffraction analysis indicates that the samples are enriched with quartz, muscovite, chlorite, sericite and albite, thus confirming the geological origin of debris mostly from local rock outcrops (a local formation of micaschist). SEM analysis (Fig. 6) revealed algae, spore, pollen and microfauna. Moreover we observed also spherical structures (Fig. 6d) characterized (from EDS analysis) by an abundance of FeO (45.3 %) and Al_2O_3 (19.8 %). This composition confirms that these structures are cenospheres (i.e. a residual product of carbon combustion, see Fig. 6

TCD
8, 3171–3206, 2014

and Kolay and Singh, 2001). These cenospheres can be carried out by a wind contribution probably from siderurgic district at the northern fringe of the Po Plain (c. more than 150 km southward the Forni Glacier), suggesting a limited allochthonous input and a human impact even at the glacier surface.

To evaluate the fine debris cover evolution, during ablation seasons 2012 and 2013 the debris coverage rate (C_r) was evaluated (see Eq. 3). From 4 July to 9 September 2012 we found a higher C_r on sites characterized by coarser dust (i.e. 96 g m^{-2} per day along an entire ablation season) than in the sites featuring finer sediment (i.e. 1 g m^{-2} per day). In the 2013 measures are more representative of the average debris cover condition of the ablation tongue of the glacier. The C_r value we found is 6 g m^{-2} per day.

As at the each field survey the parcels were not distinguishable from glacier areas nearby, the development of debris coverage resulted occurring at a fast rate. This evolution is highlighted also from the sedimentological analyses performed on the 2012 samples. During the ablation season the grain-size remains were almost similar with a slight increasing of finer sedimentological classes (i.e. silt and clay), on the other hand a more intense growing of the total organic carbon (i.e. TOC) is observed. At the beginning of July the TOC ranges from 1.6 g kg^{-1} (at sample 9a) to 26.3 g kg^{-1} (at sample 10a), at the end of the ablation period the organic carbon arises up to 41.9 g kg^{-1}. The higher values are in correspondence of finer debris (i.e. samples 9a, 9b, 9c, 11a and 11c, enriched in silt and clay), on the contrary in coarser sample 10a, 10b and 10c the TOC results lower.

The evolution of the supraglacial debris is also analysed through SEM observations. At the beginning of the melting time frame, the sediment was characterized by sharp and angular clasts; on the other hand, the samples collected in September 2012 featured more rounded shapes, suggesting a supraglacial mass transport.

TCD
8, 3171–3206, 2014

5 Discussion

To investigate the robustness of our method to quantify d and its sensitivity to changes in the chosen T_{GS}, we firstly varied the applied T_{GS} values up to ±10 % of their initial values ($T_{GS-10\%}$ and $T_{GS+10\%}$ respectively, Fig. 7): for example whenever the applied T_{GS} value to discriminate debris from bare ice was 100, we recalculated d with 90 ($T_{GS-10\%}$ obtaining $d_{-10\%}$) and with 110 ($T_{GS+10\%}$ obtaining $d_{+10\%}$). We applied this simple test to all the performed measurements (51 field data) thus obtaining 51 $d_{-10\%}$ values and 51 $d_{+10\%}$ values. Then we evaluated the departures of $d_{-10\%}$ ($d - d_{-10\%}$) from d which resulted up to −0.07 (with a mean value of −0.02). Moreover we calculated the departures of $d_{+10\%}$ ($d - d_{+10\%}$) from d which were found lower than +0.09 (with a mean value of +0.02). We found that whenever d was higher than 0.25 the $d - d_{-10\%}$ and $d - d_{+10\%}$ values reached their maxima. In fact $d - d_{-10\%}$ was −0.07 when d value was found 0.28 and $d - d_{+10\%}$ was +0.09 with a d value was equal to 0.60. Considering the whole sample it resulted that slightly more than 70 % of d featured $d - d_{-10\%}$ up to −0.02 and $d - d_{+10\%}$ lower than +0.03.

Moreover we used $d_{-10\%}$ and $d_{+10\%}$ values to look for a relation with α obtaining two new equations (reported in Table 3 together with Eq. 4). Applying these 3 equations to the d dataset it was possible to estimate glacier albedo; the modelled albedo values were compared to the albedo data obtained from field radiation measurements and the departures between the two records resulted very small, with a mean value lower than ±0.01.

This suggests that the sensitivity of our method to changes in the applied threshold is not so high to affect the reliability of the results. Moreover we also tested the method using a unique threshold value. For this attempt we applied $T_{GS\text{-}AVE}$ (i.e. 92) obtained averaging all the 51 T_{GS} values thus obtaining 51 d_{AVE} values. Then we compared these d_{AVE} values to d dataset obtained through the supervised classification (51 T_{GS} values). The obtained scatter plot (Fig. 8) indicates a not negligible relation among the two datasets thus suggesting that a unique threshold value could be sufficient to

TCD
8, 3171–3206, 2014

describe debris distribution on different images; then we applied the obtained 51 d_{AVE} values to look for a relation with α data finding the following equation:

$$\ln \alpha = (-1.38 \pm 0.21) \cdot d_{AVE} + (1.58 \pm 0.05) \quad (5)$$

Equation (5) features a R value of 0.68, meaningful but lower than the one of Eq. (4) thus suggesting that the different T_{GS} we found for each image (even if they require to spend more time in the image analysis) permit a better and detailed determination of debris distribution and then a more accurate d evaluation.

Then summarizing, to look for the most reliable relation between d and α the best and suitable solution is to apply as many specific T_{GS} values as are the images to be analysed thus describing with further details the large variability of surface conditions which affect glacier surface during the summer season.

The relation between albedo and debris cover we found underlines a strong influence driven by the glacier surface characteristics. The dust resulted featuring a high spatial (over the glacier tongue) and temporal (during the summer season) variability. In proximity of the nesting rock flanks and of the median moraine sediments are more diffuse and poorly sorted, indicating deposition after mass transport. At the end of the ice melting season a more diffuse fine debris coverage occurs on the glacier surface. Similarly to the dust distribution, the albedo variability is higher at the end of the ice melting time window as well. Other parameters affecting the fine sediment accumulation are represented by supraglacial water streams (i.e. bedieres), wind contribution, and in situ weathering of coarser clasts. Moreover, the liquid precipitation had a non-negligible effect on ice albedo but its consequence was short lasting (from 1.8 to 1 day long) thus the actual impact on other processes driven by surface albedo (like ice melt rates and magnitude) depends on frequency and duration of summer rainfall.

Regarding the debris origin, X-ray diffraction analysis indicates that the largest part of our samples was enriched with minerals which confirm the local geological origin of debris mostly from rock outcrops. Nevertheless the spherical structures characterized (from EDS analysis) by an abundance of FeO and Al_2O_3 we found through SEM

TCD
8, 3171–3206, 2014

analysis and we identified as cenospheres suggest an impact on glacier from siderurgic factories located at the northern fringe of the Po Plain.

The evolution of sedimentological properties can be evaluated sampling a same site at the beginning and at the end of ablation season. The organic content (TOC) increased during the summer time frame and its distribution was controlled by the grain-size of the supraglacial sediment. In fact TOC seems to be more abundant in finer sediments (Table 2). This can be explained by the stability of the finer debris area: it is likely that this place offers refuge for organic particles transported by wind and the environmental conditions suitable for development of algae, yeasts and bacteria. Yeasts had already been identified at the Forni Glacier surface (see Turchetti et al., 2008). Moreover, Gobbi et al. (2006) reported the presence of arthropod fauna on the surface of the Forni Glacier, which by decaying can supply significant organics.

6 Conclusions

This work represents an attempt for improving the research on fine debris coverage at the surface of debris free glaciers and for contributing to fill a knowledge gap. In fact, no systematic studies have been previously performed at the melting surface of debris free glaciers but only at snow covered areas. Moreover, dust and black carbon occurrence on glacier ice surface seems to have increased over the recent years due to the ongoing Alpine glacier shrinkage (e.g. Oerlemans et al., 2009; Diolaiuti and Smiraglia, 2010), thus requiring accurate studies to describe debris coverage, pattern and evolution and their influence on ice albedo. For this reason, we proposed a novel integrated method to describe dust and fine supraglacial debris and their effects on ice albedo. The image analysis permitted to evaluate 51 d values ranging from a 0.01 to 0.63. The measured ice albedo was found varying from 0.06 to 0.32. We investigated the robustness of our image analysis with two sensitivity tests: (i) varying the selected threshold up to ±10 % for each image and (ii) applying a unique threshold ($T_{GS\text{-}AVE}$) obtained by averaging all the chosen T_{GS}. Considering the whole sample, it resulted

TCD
8, 3171–3206, 2014

that more than 70 % of d featured $d - d_{-10\%}$ up to −0.02 and $d - d_{+10\%}$ lower than +0.03. These data suggest that the sensitivity of our method to changes in the applied threshold is not so high to affect the reliability of the results. Moreover, even if T_{GS} analysis is more time-consuming, the specific T_{GS} values found for each image permit a better and detailed determination of debris distribution and therefore a more accurate d evaluation. Then summarizing to look for the most reliable relation between d and α, the best and suitable solution is to apply a specific T_{GS} value for each image.

In 2012 we found a higher C_r (i.e. 96 g m^{-2} per day along an entire ablation season) on sites characterized by coarser dust than in the sites featuring finer sediment (i.e. 1 g m^{-2} per day). In 2013 the average debris coverage rate (C_r) of the ablation tongue of the glacier resulted equal to 6 g m^{-2} per day.

The preliminary analyses of the supraglacial debris evolution suggest a variable sediment development during the melting season assessed by rapid changes in sedimentological features and in the content of organics. The latter resulted increased during the summer time frame and its distribution is controlled by the grain size of the supraglacial sediment. In fact, TOC seems to be more abundant in correspondence with finer sediments. Moreover, the surface fine debris evolution is also forced by the occurrence of liquid precipitation. On the one hand, rainfall washes out the dust accumulation on glacier surface; but on the other hand, the rain smoothing effect on the ice surface reduces the roughness. This influence was quantified in an albedo increase up to 20 %, two days long.

Regarding the debris origin, X-ray diffraction analysis confirms that the main debris supplier are local rock outcrops (made by a local formation of micaschist). By SEM analysis we found algae, spore, pollen, microfauna and cenospheres. These latter particles can be derived from siderurgic industries of the Po Plain and then transported to the glacier surface by wind.

In conclusion, this methodological approach is applied to a very small scale (parcel of 1 m × 1 m), nevertheless it could be extended to a larger scale. For instance, the image analysis can be performed on higher resolution imagery such as orthophotos

TCD
8, 3171–3206, 2014

(for Lombardy Alps available with pixel resolution of 0.5 m × 0.5 m) or satellite imagery (featuring a resolution of 3–5 m or better). This improvement and the jump of scale will permit to distribute ice albedo once the debris properties are analysed and the relationship between albedo and debris ratio is known.

Acknowledgements. This work was conducted in the framework of the SHARE-Stelvio Project, funded by Regione Lombardia and managed by FLA (Fondazione Lombardia per l'Ambiente) and Ev-K2-CNR. The AWS1 Forni is developed under the umbrella of the SHARE Project. SHARE (Stations at High Altitude for Research on the Environment) is an international program developed and managed by the Ev-K2-CNR. The data analysis was also performed in the framework of the PRIN project 2010/2011 (2010AYKTAB_006). We are grateful to the Stelvio National Park management Staff, the municipality of Valfurva, Eraldo Meraldi, Gian Pietro Verza and Roberto Chillemi for their fundamental technical assistance on the field, to Chiara Compostella for assistance during sedimentological analyses and to Agostino Rizzi for assistance during SEM-EDS analyses.

References

Aoki, T., Aoki, T., Fukabori, M., Tachibana, Y., Zaizen, Y., Nishio, F., and Oishi, T.: Spectral albedo observation on the snow field at Barrow, Alaska, Polar Meteor. Glaciol., 12, 1–9, 1998.

Aoki, T., Motoyoshi, H., Kodama, Y., Yasunari, T. J., Sugiura, K., and Kobayashi, H.: Atmospheric aerosol deposition on snow surfaces and its effect on albedo, Sola, 2, 13–16, 2006.

Arnold, N. S., Willis, I. C., Sharp, M. J., Richards, K. S., and Lawson, W. J.: A distributed surface energy-balance model for a small valley glacier. Development and testing for Haut Glacier d'Arolla,Valais, Switzerland, J. Glaciol., 42, 77–89, 1996.

Bolch, T.: Debris, in: Encyclopedia of Snow, Ice and Glaciers, edited by: Singh, V., Singh, P., and Haritashya, U., Springer Publications, Utrecht, the Netherlands, 186–188, 2011.

Brock, B. W.: An analysis of short-term albedo variations at Haut Glacier d'Arolla, Switzerland, Geogr. Ann. A, 86, 53–65, 2004.

Brock, B. W., Willis, I. C., and Sharp, M. J.: Measurement and parameterization of albedo variations at Haut Glacier d'Arolla, Switzerland, J. Glaciol., 46, 675–688, 2000.

TCD
8, 3171–3206, 2014

Citterio, M., Diolaiuti, G., Smiraglia, C., Verza, G., and Meraldi, E.: Initial results from the automatic weather station (AWS) on the ablation tongue of Forni Glacier (Upper Valtellina, Italy), Geogr. Fis. Din. Quat., 30, 141–151, 2007.

Conway, J., Gades, A., and Raymond, C. F.: Albedo of dirty snow during conditions of melt, Water Resour. Res., 32, 1713–1718, 1996.

D'Agata, C., Bocchiola, D., Maragno, D., Smiraglia, C., and Diolaiuti, G.: Glacier shrinkage driven by climate change during half a century (1954–2007) in the Ortles-Cevedale Group (Stelvio National Park, Lombardy, Italian Alps), Theor. Appl. Climatol., 116, 169–190, doi:10.1007/s00704-013-0938-5, 2013.

Deline, P.: Change in surface debris cover on Mont Blanc massif glaciers after the "Little Ice Age" termination, The Holocene 15, 302–309, 2005.

Diolaiuti, G. and Smiraglia, C.: Changing glaciers in a changing climate: how vanishing geomorphosites have been driving deep changes in mountain landscapes and environments, Geomorphologie, 2, 131–152, 2010.

Diolaiuti, G., Smiraglia, C., Verza, G. P., Chillemi, R., and Meraldi, E.: La rete micrometeorologica glaciale lombarda: un contributo alla conoscenza dei ghiacciai alpini e delle loro variazioni recenti, in: Clima e Ghiacciai, la Crisi delle Risorse Glaciali in Lombardia, Regione Lombardia, edited by: Smiraglia, C., Morandi, G., Diolaiuti, G., Regione Lombardia, Milan, 69–92, available at: http://users.unimi.it/glaciol (last access: 5 June 2014), 2009.

Diolaiuti, G., Bocchiola, D., D'Agata, C., and Smiraglia, C.: Evidence of climate change impact upon glaciers recession within the Italian Alps: the case of Lombardy glaciers, Theor. Appl. Climatol., 109, 429–445, doi:10.1007/s00704-012-0589-y, 2012.

Flanner, M. G., Zender, C. S., Hess, P. G., Mahowald, N. M., Painter, T. H., Ramanathan, V., and Rasch, P. J.: Springtime warming and reduced snow cover from carbonaceous particles, Atmos. Chem. Phys., 9, 2481–2497, doi:10.5194/acp-9-2481-2009, 2009.

Fujita, K.: Effect of dust event timing on glacier runoff: sensitivity analysis for a Tibetan glacier, Hydrol. Process., 21, 2892–2896, 2007.

Gale, S. J. and Hoare, P. G.: Quaternary Sediments, Belhaven Press, New York, 1991.

Garavaglia, V., Pelfini, M., Diolaiuti, G., Pasquale, V., and Smiraglia, C.: Evaluating tourist perception of environmental changes as a contribution to managing natural resources in glacierized areas. A case study of the Forni Glacier (Stelvio National Park, Italian Alps), Environ. Manage., 50, 1125–1138, doi:10.1007/s00267-012-9948-9, 2012.

TCD
8, 3171–3206, 2014

Gobbi, M., De Bernardi, F., Pelfini, M., Rossaro, B., and Brandmayr, P.: Epigean Arthropod succession along a 154-year glacier foreland chronosequence in the Forni Valley (Central Italian Alps), Arct. Antarct. Alp. Res., 38, 357–362, 2006.
Hartmann, D. L.: Global Physical Climatology (International Geophysics), Academic Press, San Diego, 56, 411 pp., 1994.
Heiri, O., Lotter, A. F., and Lemcke, G.: Loss on ignition as a method for estimating organic and carbonate content in sediments: reproducibility and comparability of results, J. Paleolimnol., 25, 101–110, 2001.
ImageJ: available at: http://rsbweb.nih.gov/iJ (last access: 5 June 2014), 2004.
Irvine-Fynn, T., Bridge, J., and Hodson, A.: Rapid quantification of cryoconite: granule geometry and in situ supraglacial extents, using examples from Svalbard and Greenland, J. Glaciol., 56, 297–308, 2010.
Kirkbride, M.: Debris-covered glaciers, in: Encyclopedia of Snow, Ice and Glaciers, edited by: Singh, V., Singh, P., and Haritashya, U., Springer Publications, Utrecht, the Netherlands, 190–192, 2011.
Klok, E. J. and Oerlemans, J.: Model study of the spatial distribution of the energy and mass balance of Morteratschgletscher, Switzerland, J. Glaciol., 48, 505–518, 2002.
Klok, E. J., Greuell, J. W., and Oerlemans, J.: Temporal and spatial variation of the surface albedo of the Morteratschgletscher, Switzerland, as derived from 12 Landsat images, J. Glaciol., 49, 491–502, 2003.
Kolay, P. K. and Singh, D. N.: Physical, chemical, mineralogical, and thermal properties of cenospheres from an ash lagoon, Cement Concrete Res., 31, 539–542, 2001.
Mattson, L. E., Gardner, J. S., and Young, G. J.: Ablation on debris covered glaciers: an example from the Rakhiot Glacier, Punjab, Himalaya. IAHS Publ. 218, 289–296, 1993.
Mihalcea, C., Mayer, C., Diolaiuti, G., Lambrecht, A., and Smiraglia, C.: Ice ablation and meteorological conditions on the debris covered area of Baltoro Glacier, Karakoram (Pakistan), Ann. Glaciol., 43, 292–300, 2006.
Mihalcea, C., Mayer, C., Diolaiuti, G., D'Agata, C., Smiraglia, C., Lambrecht, A., Vuillermoz, E., and Tartari, G.: Spatial distribution of debris thickness and melting from remote-sensing and meteorological data, at debris-covered Baltoro glacier, Karakoram, Pakistan, Ann. Glaciol., 48, 49–57, 2008a.
Mihalcea, C., Brock, B. W., Diolaiuti, G., D'Agata, C., Citterio, M., Kirkbride, M. P., Cutler, M. E. J., and Smiraglia, C.: Using ASTER satellite and ground-based surface temperature

TCD
8, 3171–3206, 2014

measurements to derive supraglacial debris cover and thickness patterns on Miage Glacier (Mont Blanc Massif, Italy), Cold Reg. Sci. Technol., 52, 341–354, 2008b.
Ming, M., Xiao, C., Cachier, H., Qin, D., Qin, X., Li, Z., and Pu, J.: Black Carbon (BC) in the snow of glaciers in West China and its potential effects on albedos, Atmos. Res., 92, 114–123, 2009.
Montrasio, A., Berra, F., Cariboni, M., Ceriani, M., Deichmann, N., Ferliga, C., Gregnanin, A., Guerra, S., Guglielmin, M., Jadoul, F., Longhin, M., Mair, V., Mazzoccola, D., Sciesa, E., and Zappone, A.: Note illustrative della Carta Geologica d'Italia: foglio 024, Bormio, ISPRA, Servizio Geologico d'Italia, Roma, 2008.
Motoyoshi, H., Aoki, T., Hori, M., Abe, O., and Mochizuki, S.: Possible effect of anthropogenic aerosol deposition on snow albedo reduction at Shinjo, Japan, J. Meteorol. Soc. Jpn, 83A, 137–148, 2005.
Nakawo, M. and Young, G. J.: Field experiments to determine the effect of a debris layer on ablation of glacier ice, Ann. Glaciol., 2, 85–91, 1981.
Nakawo, M. and Young, G. J.: Estimate of glacier ablation under a debris layer from surface temperature and meteorological variables, J. Glaciol., 28, 29–34, 1982.
Nakawo, M. and Rana, B.: Estimation of ablation rate of glacier ice under a supraglacial debris layer, Geogr. Ann. A, 41, 228–230, 1999.
Nicholson, L. and Benn, D.: Calculating ice melt beneath a debris layer using meteorological data, J. Glaciol., 52, 463–470, 2006.
Oerlemans, J.: The microclimate of valley glaciers, Utrecht university Ed., Utrecht, 2010.
Oerlemans, J., Giesen, R. H., and Van Den Broeke, M. R.: Retreating alpine glaciers: increased melt rates due to accumulation of dust (Vadret da Morteratsch, Switzerland), J. Glaciol., 55, 729–736, 2009.
Østrem, G.: Ice melting under a thin layer of moraine and the existence of ice cores in moraine ridges, Geogr. Ann. A, 41, 686–694, 1959.
Painter, T. H., Flanner, M. G., Kaser, G., Marzeion, B., Van Curen, R. A., and Abdalati, W.: End of the Little Ice Age in the Alps forced by industrial black carbon, P. Natl. Acad. Sci. USA, 110, 15216–15221, 2013.
Paul, F. and Kääb, A.: Perspectives on the production of a glacier inventory from multispectral satellite data in the Canadian Arctic: Cumberland Peninsula, Baffin Island, Ann. Glaciol., 42, 59–66, 2005.

TCD
8, 3171–3206, 2014

Paul, F., Kääb, A., and Haeberli, W.: Recent glacier changes in the Alps observed from satellite: consequences for future monitoring strategies, Global Planet. Change, 56, 111–122, 2007.
Qian, Y., Flanner, M. G., Leung, L. R., and Wang, W.: Sensitivity studies on the impacts of Tibetan Plateau snowpack pollution on the Asian hydrological cycle and monsoon climate, Atmos. Chem. Phys., 11, 1929–1948, doi:10.5194/acp-11-1929-2011, 2011.
Ramanathan, V.: Role of Black Carbon in Global and Regional Climate Change, Testimonial to the House Committee on Oversight and Government Reform, 18 October 2007, available at: http://www-ramanathan.ucsd.edu/files/brt20.pdf (last access: 5 June 2014), 2007.
Sakai, A., Takeuchi, N., Fujita, K., and Nakawo, M.: Role of supraglacial ponds in the ablation process of a debris-covered glacier in the Nepal Himalayas, IAHS-AISH P., 264, 119–130, 2000.
Senese, A., Diolaiuti, G., Mihalcea, C., and Smiraglia, C.: Meteorological evolution on the ablation zone of Forni Glacier, Ortles-Cevedale Group (Stelvio National Park, Italian Alps) during the period 2006–2008, Bollettino della Società, Roma, Serie XIII, vol. III, fascicolo 4, Boll. Soc. Geogr. Ita., 3, 845–864, 2010.
Senese, A., Diolaiuti, G., Mihalcea, C., and Smiraglia, C.: Energy and mass balance of Forni Glacier (Stelvio National Park, Italian Alps) from a 4-year meteorological data record, Arct. Antarct. Alp. Res., 44, 122–134, doi:10.1657/1938-4246-44.1.122, 2012a.
Senese, A., Diolaiuti, G., Verza, G. P., and Smiraglia, C.: Surface energy budget and melt amount for the years 2009 and 2010 at the Forni Glacier (Italian Alps, Lombardy), Geogr. Fis. Din. Quat., 35, 69–77, 2012b.
Sodemann, H., Palmer, A. S., Schwierz, C., Schwikowski, M., and Wernli, H.: The transport history of two Saharan dust events archived in an Alpine ice core, Atmos. Chem. Phys., 6, 667–688, doi:10.5194/acp-6-667-2006, 2006.
Takeuchi, N.: Surface albedo and characteristics of cryoconite on an Alaska glacier (Gulkana Glacier in the Alaska Range), Bull. Glaciol. Res., 19, 63–70, 2002.
Takeuchi, N., Kohshima, S., Yoshimura, Y., Seko, K., and Fujita, K.: Characteristics of cryoconite holes on a Himalayan glacier, Yala Glacier Central Nepal, Bull. Glaciol. Res., 17, 51–59, 2000.
Takeuchi, N., Kohshima, S., and Seko, K.: Structure, formation, darkening process of albedo reducing material (cryoconite) on a Himalayan glacier: a granular algal mat growing on the glacier, Arct. Antarct. Alp. Res., 33, 115–122, 2001.

TCD
8, 3171–3206, 2014

Takeuchi, N., Matsuda, Y., Sakai, A., and Fujita, K.: A large amount of biogenic surface dust (cryoconite) on a glacier in the Qilian Mountains, China, Bull. Glaciol. Res., 22, 1–8, 2005.
Tangborn, W. and Rana, B.: Mass balance and runoff of the partially debris-covered Langtang Glacier, Nepal, IAHS-AISH P., 264, 99–108, 2000.
Turchetti, B., Buzzini, P., Goretti, M., Branda, E., Vaughan-Martini, A., Diolaiuti, G., D'Agata, C., and Smiraglia, C.: Psychrophilic yeasts in glacial environments of Alpine glaciers, FEMS Microbiol. Ecol., 63, 73–83, doi:10.1111/j.1574-6941.2007.00409.x, 2008.
Walkley, A. and Black, I. A.: An examination of Degtjareff method for determining soil organic matter and a proposed modification of the chromic acid titration method, J. Soil Sci., 37, 29–38, 1934.
Wentworth, C. K.: A scale of grade and class terms for clastic sediments, J. Geol., 30, 377–392, 1922.
World Meteorological Organization: Guide to meteorological instruments and method of observation, Seventh edition, Geneve, 2008.
Yasunari, T. J., Bonasoni, P., Laj, P., Fujita, K., Vuillermoz, E., Marinoni, A., Cristofanelli, P., Duchi, R., Tartari, G., and Lau, K.-M.: Estimated impact of black carbon deposition during pre-monsoon season from Nepal Climate Observatory – Pyramid data and snow albedo changes over Himalayan glaciers, Atmos. Chem. Phys., 10, 6603–6615, doi:10.5194/acp-10-6603-2010, 2010.

TCD
8, 3171–3206, 2014

Table 1. Influence of rainfall on surface albedo (α) measured from the AWS1 Forni. In the table are reported the 30 rainy events that occurred in 2011, 2012 and 2013 ablation seasons and the albedo values before, during and after every rainfall.

Before rainy event		During rainy event		After rainy even		Albedo increasing
Data	α	Data	α	Data	α	%
16 Jun 11	0.33	17–18 Jun 11	0.21	19 Jun 11	0.41	24.2
20 Jun 11	0.31	21–23 Jun 11	0.21	24 Jun 11	0.31	0.0
24 Jun 11	0.31	25–26 Jun 11	0.20	27 Jun 11	0.32	3.2
28 Jun 11	0.18	29 Jun 11	0.18	30 Jun 11	0.20	11.1
3 Jul 11	0.23	4–8 Jul 11	0.20	9 Jul 11	0.25	8.7
2 Aug 11	0.20	3 Aug 11	0.19	4 Aug 11	0.24	20.0
31 Aug 11	0.25	1 Sep 11	0.25	2 Sep 11	0.28	12.0
2 Sep 11	0.28	3–6 Sep 11	0.24	7 Sep 11	0.29	3.6
7 Sep 11	0.29	8 Sep 11	0.22	9 Sep 11	0.31	6.9
11 Sep 11	0.22	12 Sep 11	0.23	13 Sep 11	0.25	13.6
19 Jun 12	0.20	20–26 Jun 12	0.21	27 Jun 12	0.22	10.0
1 Jul 12	0.17	2–7 Jul 12	0.22	8 Jul 12	0.19	11.8
8 Jul 12	0.19	9–11 Jul 12	0.19	12 Jul 12	0.23	21.0
12 Jul 12	0.23	13–15 Jul 12	0.20	16 Jul 12	0.29	26.1
19 Jul 12	0.20	20–22 Jul 12	0.24	22 Jul12	0.27	35.0
23 Jul 12	0.21	24–25 Jul 12	0.20	26 Jul 12	0.22	4.8
26 Jul 12	0.22	27–31 Jul 12	0.20	1 Aug 13	0.23	4.5
2 Aug 12	0.20	3–6 Aug 12	0.18	7 Aug 12	0.24	20.0
24 Aug 12	0.16	25–26 Aug 12	0.19	27 Aug 12	0.26	62.5
23 Sep 12	0.22	24–27 Sep 12	0.23	28 Sep12	0.32	45.4
28 Sep 12	0.32	29 Sep–2 Oct 12	0.24	3 Oct 12	0.32	0.0
6 Oct 12	0.27	7 Oct 12	0.23	8 Oct 12	0.30	11.1
16 Jul 13	0.16	17–24 Jul 13	0.18	25 Jul 13	0.17	6.3
25 Jul 13	0.17	26 Jul 13	0.16	27 Jul 13	0.18	5.9
28 Jul 13	0.16	29 Jul 13	0.15	30 Jul 13	0.23	43.7
30 Jul 13	0.23	31 Jul 13	0.19	1 Aug 13	0.25	8.7
6 Aug 13	0.16	7–9 Aug 13	0.16	10 Aug 13	0.26	62.5
12 Aug 13	0.19	13–15 Aug 13	0.19	16 Aug 13	0.24	26.3
31 Aug 13	0.18	1 Sep 13	0.18	2 Sep 13	0.24	33.3
26 Sep 13	0.16	27 Sep 13	0.15	28 Sep 13	0.24	50.0
MEAN	0.22		0.20		0.26	21.3

TCD
8, 3171–3206, 2014

Table 2. Properties of sites sampled for sedimentological analyses and results. The grain-size classes are referred to Krumbein's scale (Wentworth, 1922). With the asterisk it is indicated a debris sample not enough to grain size analysis.

Sample	Sampling Date	Description	Gravel (%)	Sand (%)	Silt (%)	Clay (%)	TOC ($g\,kg^{-1}$)	Weight (g)
1	30 Jun 11	Central tongue	2.1	17.4	58.8	12.3	2.7	–
2	30 Jun 11	Eastern tongue	6.6	69.7	19.6	0.6	0.6	–
3	30 Jun 11	Median moraine (5 cm thick debris)	18.9	50.2	24.3	4.5	1.6	–
4	30 Jun 11	Central tongue, predominantly bare ice	0.4	29.4	30.9	15.8	3.6	–
5	30 Jun 11	Central tongue, cryoconite	5.6	32.9	30.9	15.8	5.1	–
6	30 Jun 11	Eastern tongue	0.1	14.5	35.3	20.5	5.0	–
7	25 Aug 11	Eastern tongue	6.2	72.4	15.7	3.4	1.9	–
8	25 Aug 11	Eastern tongue	0.1	21.4	31.7	22.8	5.9	–
9a	4 Jul 12	Central tongue	19.7	66.3	8.9	2.2	1.6	67.7
10a	4 Jul 12	Central tongue	8.6	33.6	25.7	12.3	26.3	1559.4
11a	4 Jul 12	Eastern tongue	0.1	17.7	35.5	19.7	18.3	432.0
9b	7 Aug 12	Central tongue, the same site of sample 9a	13.0	75.0	7.4	2.1	1.3	11.9
10b	7 Aug 12	Central tongue, the same site of sample 10a	–	–	–	–	40.8	4026.9
9c	9 Sep 12	Central tongue, the same site of samples 9a and 9b	22.5	66.3	7.9	2.3	5.4	49.4
10c	9 Sep 12	Central tongue, the same site of samples 10a and 10b	2.4	23.6	40.9	16.7	38.1	2356.7
11c	9 Sep 12	Eastern tongue, the same site of sample 11a	2.6	25.4	35.2	14.9	41.9	462.4
12a	11 Jul 13	Central tongue	–	–	–	–	–	29.1
12b	31 Jul 13	Central tongue, the same site of sample 12a	–	–	–	–	–	159.5
12c	6 Sep 13	Central tongue, the same site of sample 12a and12b	–	–	–	–	–	308.3
12d	4 Oct 13	Central tongue, the same site of sample 12a, 12b and 12c	–	–	–	–	–	59.5

TCD
8, 3171–3206, 2014

Table 3. Depending on the 3 different ratio datasets (considering $d_{+10\%}$, $d_{-10\%}$, and d) the differences between measured (α_M) and calculated (α_C) albedo data are shown.

Relation equation	Min ($\alpha_M - \alpha_C$)	Mean ($\alpha_M - \alpha_C$)	Max ($\alpha_M - \alpha_C$)
$\ln(\alpha) = (-2.20 \pm 0.21) d_{-10\%} + (-1.52 \pm 0.04)$	−0.06	+0.011	+0.13
$\ln(\alpha) = (-2.04 \pm 0.19) d + (-1.50 \pm 0.04)$	−0.07	+0.005	+0.12
$\ln(\alpha) = (-1.89 \pm 0.17) d_{+10\%} + (-1.48 \pm 0.04)$	−0.07	−0.001	+0.12

TCD
8, 3171–3206, 2014

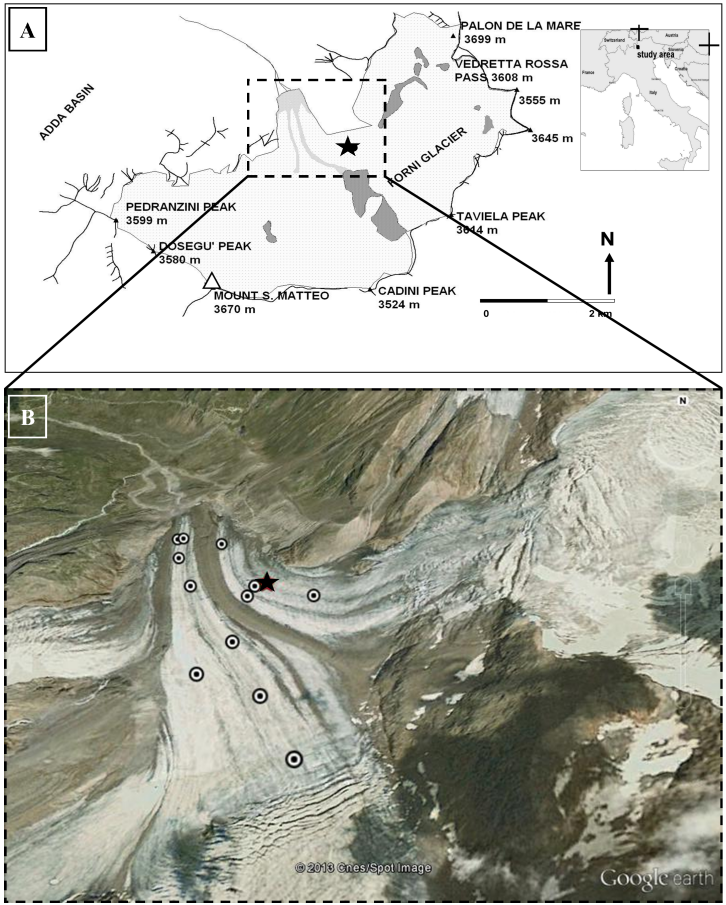

Figure 1. (a) The position of Forni Glacier in the Italian Alps and of AWS1 Forni (black star, in both panels). **(b)** Enlarged view of the Forni Glacier (image credit: GoogleEarth™) showing the location of field measurements (black dots).

TCD
8, 3171–3206, 2014

Figure 2. Series of pictures illustrating: **(a)** sampling supraglacial debris, **(b)** measuring albedo and **(c)** acquiring high resolution digital images of the glacier surface.

TCD
8, 3171–3206, 2014

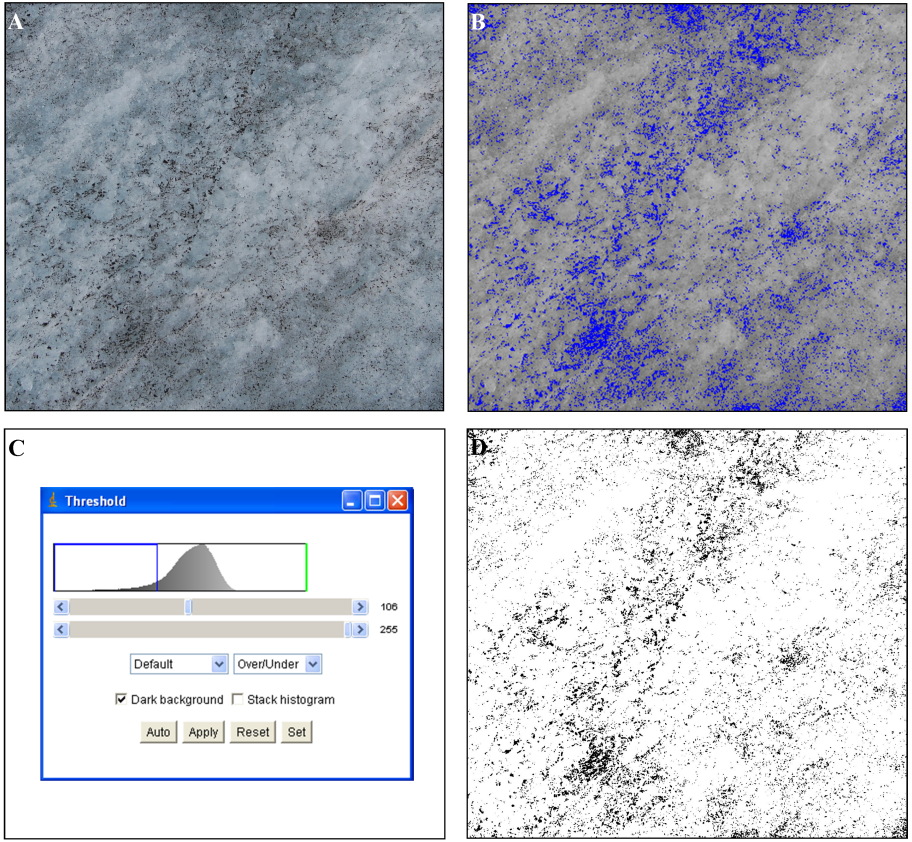

Figure 3. Example of the procedure followed in image analysis: **(a)** original cut frame; **(b)** 8 bit conversion and discrimination between the debris-covered (in blue) and debris-free ice surface; **(c)** definition of the threshold; **(d)** calculated debris covered ratio.

TCD
8, 3171–3206, 2014

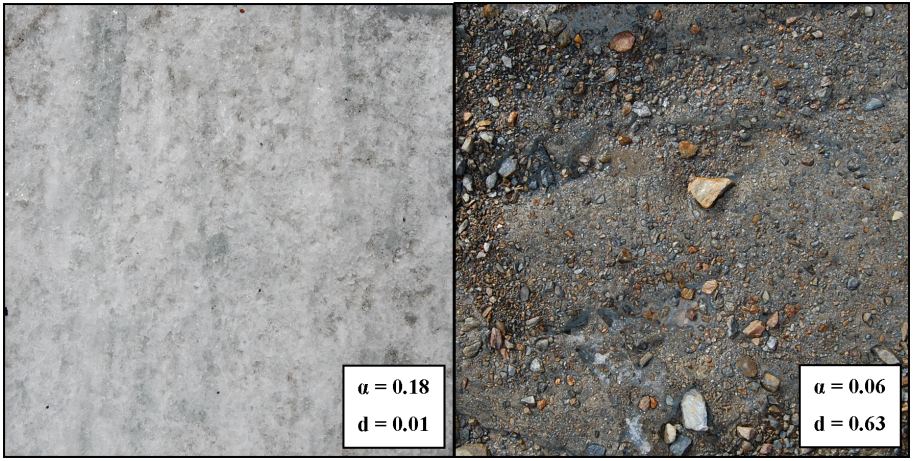

Figure 4. Examples of Forni Glacier surfaces: albedo (α) and debris cover ratio (d) values are shown.

TCD
8, 3171–3206, 2014

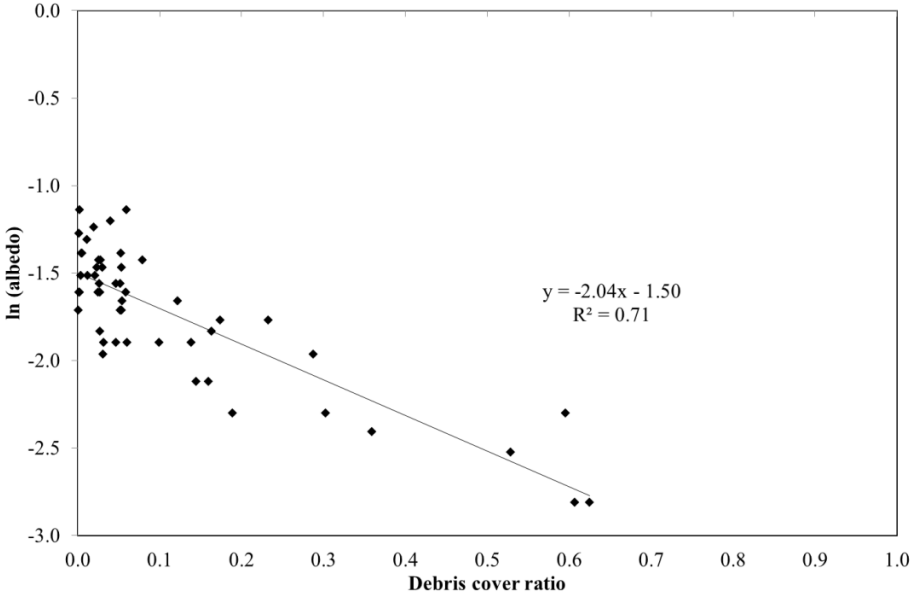

Figure 5. Albedo natural logarithm values vs. debris cover ratio (2011–2013 data).

TCD
8, 3171–3206, 2014

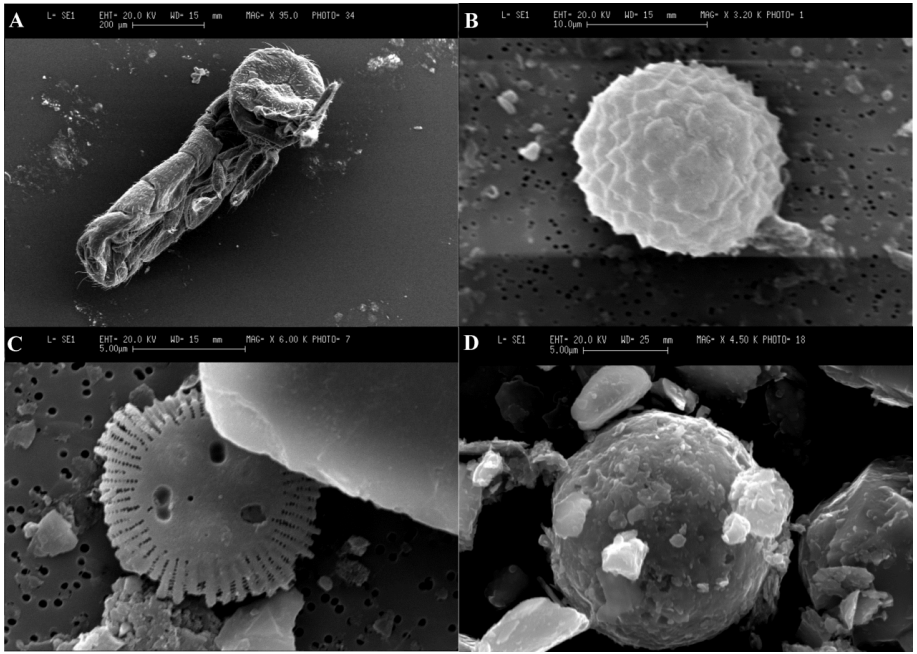

Figure 6. SEM investigation on bulk samples from Forni Glacier evidenced the presence of **(a)** organism of collembolan order, **(b)** spore, **(c)** diatom and **(d)** cenosphere (a residual product of carbon combustion).

TCD
8, 3171–3206, 2014

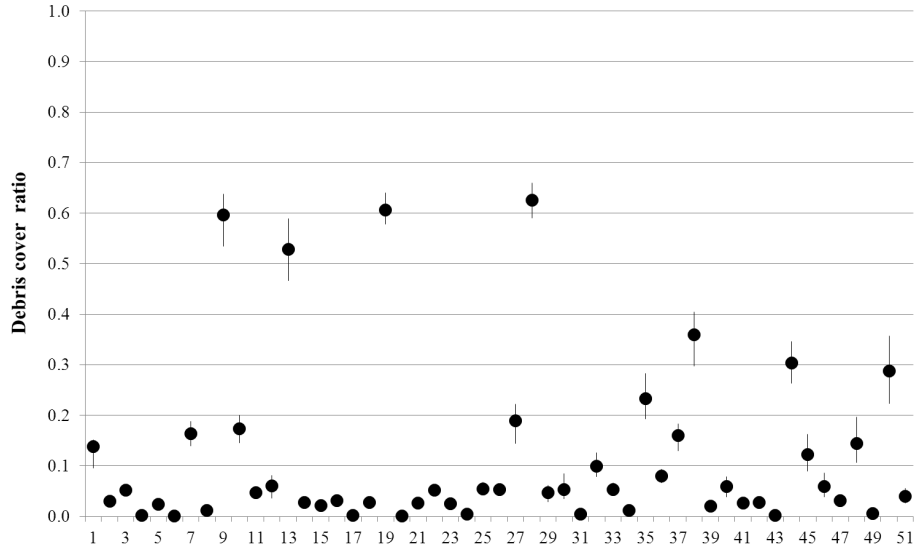

Figure 7. Values of d from 51 measurements performed in 2011, 2012 and 2013 ablation seasons (black dots). The vertical bars indicate the $d_{+10\%}$ and $d_{-10\%}$ values.

TCD
8, 3171–3206, 2014

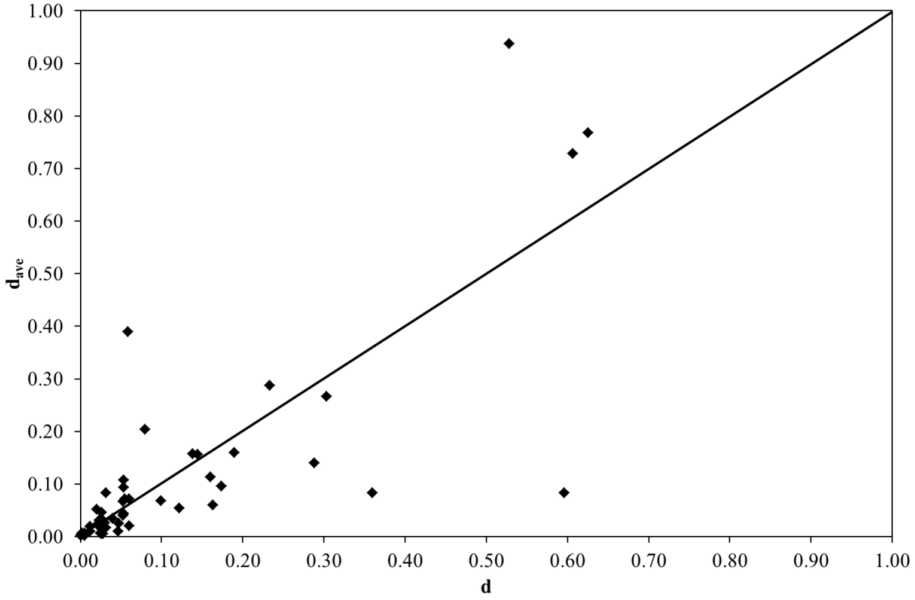

Figure 8. Scatter plot reporting d (obtained from T_{GS}) vs. d_{AVE} (obtained from $T_{GS\text{-}AVE}$) values.

TCD
8, 3171–3206, 2014